Ligand-free synthesis of tunable size Ln:$BaGdF_5$ (Ln= Eu^{3+} and Nd^{3+}) nanoparticles: Luminescence, magnetic properties, and biocompatibility.

Ana I. Becerro,[1] Daniel González-Mancebo,[1] Eugenio Cantelar[2], Fernando Cussó,[2] Grazyna Stepien,[3] Jesús M. de la Fuente,[4] and Manuel Ocaña[1]

[1]*Instituto de Ciencia de Materiales de Sevilla (CSIC-US). c/ Américo Vespucio, 49, 41092 Seville (Spain).*

[2]*Dpto. Física de Materiales, C-04. Universidad Autónoma de Madrid, 28049 Madrid (Spain).*

[3] *Instituto de Nanociencia de Aragón, Universidad de Zaragoza. c/ Mariano Esquilor s/n. 50018 Zaragoza (Spain)*

[4]*Instituto de Ciencia de Materiales de Aragon, CSIC/University of Zaragoza, C/ Pedro Cerbuna, 12. 50009 Zaragoza (Spain)*

Abstract

Bifunctional and highly uniform Ln:$BaGdF_5$ (Ln= Eu^{3+} and Nd^{3+}) nanoparticles have been successfully synthesized using a solvothermal method consisting in the aging at 120 °C of a glycerol solution containing the corresponding Lanthanide acetylacetonates and butylmethylimidazolium tetrafluoroborate. The absence of any surfactant in the synthesis process rendered hydrophilic nanospheres (with tunable diameter from 45 nm 85 nm, depending on the cations concentration of the starting solution) which are suitable for bioapplications. The particles are bifunctional because they showed both optical and magnetic properties due to the presence of the optically active lanthanides (Eu^{3+} in the visible and Nd^{3+} in the NIR regions of the electromagnetic spectrum) and the paramagnetic gadolinium ion, respectively. The luminescence decay curves of the nanospheres doped with different amounts of Eu^{3+} and Nd^{3+} have been recorded in order to determine the optimum dopant concentration in each case, which resulted to be 5% Eu^{3+} and 0.5% Nd^{3+}. Likewise, proton relaxation times were measured at 1.5 T in water suspensions of the optimum particles found in the luminescence study. The values obtained suggested that both kinds of particles could be used as positive contrast agents for MRI. Finally, it was demonstrated that both the 5% Eu^{3+} and 0.5% Nd^{3+}-doped $BaGdF_5$ nanospheres showed negligible cytotoxicity for VERO cells for concentrations up to 0.25 mg mL^{-1}.

1.- Introduction

In recent years, lanthanide-doped rare earth fluoride nanoparticles have become a research focus in the optical materials and biomedical fields because of their interesting luminescent properties which confer to them important applications as components of different optoelectronic devices and as biosensors and optical bioprobes.[1,2,3,4,5] In comparison with oxygen-based systems, fluorides possess very low vibrational energies and therefore the quenching of the excited states of the lanthanide (Ln^{3+}) ions is minimal, thus improving their luminescence emissions.[6,7] Among the fluoride systems, the Ln:GdF_3 and Ln:$MGdF_x$ compositions (Ln= optically active lanthanide ion; M= group I or II element with x= 4 or 5 respectively) show an added value because of the large magnetic moment and nanoseconds electronic relaxation time of Gd^{3+}, which makes them ideal paramagnetic relaxation agents to be used in magnetic resonance imaging (MRI).[8,9]

Up to now, high quality, monodisperse, Ln-doped GdF_3 as well as $MGdF_4$ (M= alkaline element) nanoparticles including $LiGdF_4$,[10] $NaGdF_4$,[11] and $KGdF_4$,[12] with controllable phase, size and shape, have been reported in the literature. However, the $MGdF_5$ (M= earth alkaline element) systems have been paid much less attention in spite of the fact that Yb^{3+}/Er^{3+}:$BaGdF_5$ nanocrystals have been shown to be as efficient as β-$NaYF_4$, which is considered to be the most efficient up-converting material.[13] The synthesis methods reported up to now to obtain $BaGdF_5$ particles were based, mainly, on the homogeneous precipitation, at temperatures ≥180°C during long reaction times (~24 hours), of ions from aqueous or ethylene glycol solutions containing either nitrates or chlorides as the Gd^{3+} and Ba^{2+} precursors, and $NaBF_4$ or NH_4F as the fluoride source. Most of them made use of organic additives as surfactants and led either to ill-defined, and/or poorly dispersed nanoparticles (12 – 75 nm),[14,15,16,17] although in a few cases uniform particles were obtained but their size was above 100 nm.[18,19] Only the use of oleic acid as capping agent led to monodispersed $BaGdF_5$ nanospheres (3 to 10 nm).[13,20] However, the latter method required the use of very high temperatures (300 ºC) and rendered hydrophobic particles due to the oleate ligands attached to their surface.

Herein, we propose a surfactant-free method to obtain hydrophilic, uniform $BaGdF_5$ nanoparticles with control size (45 nm to 85 nm) using lower temperatures and times than those previously reported. The method is based on a homogeneous precipitation

using suitable precursors that release cations and anions into the reaction medium in a control manner. We have used in particular gadolinium acetylacetonate as the Gd precursor and an ionic liquid (1-butyl, 3-methylimidazolium tetrafluoroborate, [BMIM]BF_4, as the fluoride source. The latter has been shown to be successful for the synthesis of homogeneous rare-earth fluoride nanoparticles, such as YF_3[21] and GdF_3,[22] because, it did not only act as a fluoride source but also as a morphology-directing agent. Likewise, glycerol has been selected as solvent because of its high viscosity, which is expected to slow down the kinetics of the process, thus favoring the formation of small, uniform particles.[23] Homogeneous precipitation requires a precise control of the experimental conditions to obtain monodisperse particles. For this reason, we have analyzed the influence of the precursors type and concentration, the solvent nature and the reaction temperature on the morphology of the precipitated particles. The crystal structure of $BaGdF_5$ has been analyzed in detail with the help of X-ray diffraction and Rietveld refinement, and compared with data of the literature. The same method is shown to be successful to obtain Eu^{3+}-doped and Nd^{3+}-doped nanophosphors with the same morphological features as the undoped particles. The reasons to select these two lanthanides as doping ions are as follows: The luminescence of Eu^{3+} is located in the red region of the electromagnetic spectrum, where the auto-fluorescence of tissues is minimal,[24] while Nd^{3+} is excited and emits within the second biological window (1000-1400 nm), in which the radiation is weakly attenuated by tissues and can penetrate more deeply than the visible light thus improving the sensitivity of the assays.[25] In both cases, particles with different doping levels were synthesized to find the optimum composition. Finally, the magnetic relaxivity as well as the cytotoxicity of the optimum Eu^{3+} and Nd^{3+}-doped particles were evaluated to assess their suitability for biomedical diagnosis.

2. Experimental section

2.1. Synthesis of samples

The $BaGdF_5$ nanoparticles were obtained according to the following method: barium nitrate ($Ba(NO_3)_2$, Sigma Aldrich, ≥ 99%) and Gadolinium acetylacetonate ($Gd(acac_3)$) hydrate ($Gd(C_5H_7O_2)_3 \cdot xH_2O$, Sigma Aldrich, 99.9%) were dissolved, with magnetic stirring at 70 °C, in 4 mL of glycerol (Gly, Panreac) to obtain a 0.04 M solution of each

cation. The solution was then cooled down to room temperature and admixed with 2 mL of a 1-butyl-3-methylimidazolium tetrafluoroborate ([BMIM]BF_4, Aldrich, ≥ 97%) solution in glycerol (0.55 M) and magnetically stirred for 5 minutes at room temperature to favor homogenization. The final solution was aged for 10 hours in tightly closed test tubes using an oven preheated at 120 °C. The resulting dispersion was cooled down to room temperature, centrifuged to remove the supernatants and washed, twice with ethanol and once with double distilled water. For some analyses, the powders were dried at room temperature. Different Gd^{3+} and F^- sources were used to analyze their effect on the particles characteristics. Such sources were $Gd(NO_3)_3$ (Sigma Aldrich, 99.99%) and NH_4F (Sigma Aldrich, 99.99%), for Gd and F, respectively. We also used solvents other than glycerol, such as ethylene glycol (EG, Sigma Aldrich, 99.99%) and butylene glycol (Fluka, 99.5%), to analyze the effect of the polyol nature on the particles morphology.

The Eu^{3+}-doped particles were synthesized following the same procedure and using Eu^{3+} acetylacetonate hydrate ($Eu(C_5H_7O_2)_3 \cdot xH_2O$, Sigma Aldrich, 99.9%) in variable amounts. The lanthanide ions (Gd + Eu) concentration was kept constant (0.04 $mol \cdot dm^{-3}$) in all experiments, whereas the Eu/(Gd + Eu) molar ratio was varied from 0.5% to 30% in order to investigate the effect of this parameter on the morphological and luminescent properties of the precipitated particles. Secondly, Nd^{3+}-doped particles were prepared to obtain a luminescent nanomaterial with Vis→IR downconversion properties. The same synthesis method described for the case of the Eu-doping was also used to obtain the Nd^{3+}-doped particles. In this case, the Nd/(Gd + Nd) molar ratio was varied from 0.5% to 1.5%.

2.2. Characterization techniques

The shape and size of the particles was examined by both *transmission electron microscopy* (*TEM*, Philips 200CM) and *scanning electron microscopy* (*SEM-FEG* Hitachi S4800). Particle size distributions were obtained from the micrographs by counting several hundreds of particles, using the free software *ImageJ*. Additional information on the size and colloidal stability of the particles in aqueous suspension (0.5 $mg \cdot mL^{-1}$ of solid) was obtained from *Dynamic Light Scattering* (*DLS*) measurements. The experiments were carried out using a Malvern Zetasizer Nano-ZS90 equipment, which was used as well to measure the Zeta potential of the suspensions.

The crystalline structure of the prepared particles was assessed by *X-ray diffraction (XRD)* using a Panalytical, X´ Pert Pro diffractometer (CuKα) with an X-Celerator detector over an angular range of 10° < 2θ < 120°, 2θ step width of 0.02°, and 10 s counting time. The crystallite size was calculated using the Scherrer formula from the full width at half maximum of a single reflection. A shape factor of k = 0.9 and an instrumental broadening factor of 0.112 were used for the calculation.

The incorporation of Ln^{3+} (Eu^{3+} and Nd^{3+}) into the $BaGdF_5$ crystal structure was proved by determination of unit cell parameters of the undoped and the Ln^{3+}-doped particles. For this purpose, the corresponding XRD patterns were analyzed using the Rietveld method with the TOPAS software (TOPAS version 4.2, Bruker AXS, 2009). Starting crystallographic parameters were taken from those reported for cubic $BaYF_5$[26] because the $BaGdF_5$ structure has not been reported in the literature. Nominal Ln^{3+} contents were added to the structure. Refined parameters were: scale factor, zero error, background coefficients, unit cell parameters and atomic displacement factors of the heavy atoms (Ba, Gd, and Ln).

The *excitation and emission spectra* of the Eu^{3+}-doped $BaGdF_5$ particles, dispersed in water (2.5 $mg \cdot mL^{-1}$), were measured in a Horiba Jobin Yvon spectrofluorimeter (Fluorolog3). The excitation/emission slits used to record the excitation and emission spectra were 1 nm/5 nm and 5nm/1nm, respectively. All the spectra were recorded using 1 nm steps. The emission spectra were transformed to the CIE color coordinates system using a 2° observer.

The *excitation and emission spectra* of the Nd^{3+}-doped $BaGdF_5$ particles, in powder form, were recorded using a cw Ti-zaphire laser (Spectra Physics).

All luminescence spectra (emission & excitation) have been corrected to account for the spectral response of the experimental setup.

Lifetime measurements were obtained under pulsed excitation at 532 nm using the second harmonics of a Nd:YAG laser (Spectra Physics model DCR 2/2A 3378) with a pulse width of 10 ns and a repetition rate of 10 Hz. Fluorescence was analyzed through an ARC monochromator model SpectraPro 500-i and then detected synchronously with an EMI-9558QB photomultiplier and recorded by a Tektronix TDS420 digital oscilloscope.

^{1}H NMR relaxation times T1 and T2 were measured at 1.5 Tesla in a Relaxiometer (Bruker Minispec spectrometer) at different concentrations of Gd^{3+} (0.2, 0.4, 0.6, 0.8, and 1.0 mmol dm^{-3}) in water at 298 K. T1 and T2 values were determined by the inversion-recovery method and by the Carr–Purcell–Maiboom–Gill sequence, respectively. Relaxivities (r_1, r_2) were obtained from the slopes of the curves 1/T1 or 2 *vs*. the concentration of Gd^{3+} expressed in mM.

2.3. Cytotoxicity assay

Vero cell cultures (monkey kidney epithelial cells) were cultured in Dulbecco's Modified Eagle's Medium (DMEM), supplemented with 10% fetal bovine serum (FBS), 5% glutamine (200 mM) and 5% penicillin (5000 units per mL)/streptomycin (5 mg mL−1). Cell cultures were incubated at 37 °C and equilibrated in 4% CO_2 and air. Cell viability and proliferation were analyzed by the MTT colorimetric assay. For the cytotoxicity assay 5000 cells were seeded in each well of 96-well plates and grown for 24 h. After that, the medium was replaced with fresh medium containing the different types of nanoparticles in varying concentrations. After cultivation again for 24 h or 120 h (in the case of 120 h, the medium was supplemented with FBS (20 μL per well) after 72 h of incubation), 20 μL of MTT dye solution (5 mg cm−3 in PBS) was added to each well. After 4 h of incubation at 37 °C and 5% CO_2, the medium was removed, the cells were washed with fresh medium, and formazan crystals were dissolved in 100 μL of DMSO. The absorbance of each well was read on a microplate reader (Biotek ELX800) at 570 nm. The spectrophotometer was calibrated to zero absorbance using culture medium without cells. The relative cell viability (%) related to control wells containing cell culture medium without nanoparticles was calculated by [A]test/[A]control × 100. Each measurement was repeated at least five times to obtain the mean values and the standard deviation.

3.- Results

3.1.- Synthesis strategy and morphology of the precipitated $BaGdF_5$ nanoparticles.

The well-known La Mer and Dinegar[27] model establishes that separation of nucleation and growth processes are necessary to obtain monodisperse particles by homogeneous precipitation while the presence of several nucleation events would obviously drive to

polydisperse systems. This requirement can be achieve through a precise control of the experimental conditions which affect the precipitation kinetics.[28] In our case, uniform and disperse nanoparticles with spherical shape (40(5) nm) were obtained after aging, at 120 °C for 10 hours in a conventional oven, 4 mL of a solution containing $Gd(acac)_3$ (0.12 M) and $Ba(NO_3)_3$ (0.12 M) in glycerol admixed with 2 mL of a glycerol solution of $[BMIM]BF_4$ (0.55 M), as illustrated in Figure 1 (top). The hydrodynamic diameter measured by DLS in a fresh aqueous suspension of the particles was 55 nm (Figure 1, middle). This value is only slightly larger than the mean particle size estimated from the TEM micrographs of the sample, and confirmed the absence of particle aggregation in the aqueous suspension.

Changing anyone of the experimental conditions necessary to obtain the particles shown in Figure 1 (top) and keeping the other conditions constant, led to the loss of the dispersion, uniformity and/or morphology of the particles. For example, using diethylene glycol (Fig. S1a) or ethylene glycol (Fig. S1b) instead of glycerol led to ill-defined precipitated or aggregated and polydispersed nanospheres, respectively. This effect can be attributed to the change in the viscosity and in the dielectric constant of the solvent. These two parameters affect, respectively, the ion diffusion, involved in the nucleation and growth processes, and the surface charge of the precipitated particles, and control therefore their aggregation. Likewise, changing the Gd^{3+} or fluoride sources to precursors that do not allow a control release of ions ($Gd(NO_3)_3$ and NH_4F) led to the formation of irregular particles with different degrees of aggregation, as shown in the TEM micrographs of Figures S1c and S1d. This result indicates that a controlled release of both the cations and anions is required to achieve the adequate reaction kinetics in this particular case. The aging temperature was also shown to be an important factor for the synthesis of uniform nanoparticles, as shown in Figures S1e and S1f, which exhibit the aggregated nanoparticles obtained at 85 °C and 180 °C, respectively. These changes must be assigned to variations in the kinetic of precipitation which also affect the nucleation and growth processes.[27]

The only experimental parameter that did not alter the shape and uniformity of the precipitated particles was the concentration of cations (Gd^{3+} and Ba^{2+}), as long as the Gd/Ba ratio was kept constant and equal to 1. However, a significant and exponential increase in the particle size up to 85 nm was observed with decreasing the cations concentration from 0.12 M to 0.02 M (Figure 1, bottom). At cations concentrations

higher than 0.12 M the particles appeared much less uniform both in size and shape, while at concentrations lower than 0.02 M no precipitate was detected after 20 hours reaction. This finding suggests that an increase in reagents concentration produces an associated increase in the number of nuclei leading to a decrease in the final particle size, in agreement with the classical model proposed by La Mer and Dinegar.[27]

In summary, tunable-size (40-85 nm), uniform, and well dispersed spherical nanoparticles can be obtained with the synthesis method reported here, as long as a strict control of the reaction parameters is applied.

The smallest particles obtained in this study (40(5) nm diameter), will be used thereafter to analyze their chemical nature, crystal structure, optical and magnetic properties as well as cytotoxicity, because their small size make them potentially useful for biological applications.[29]

3.2.- Crystal structure of the $BaGdF_5$ nanoparticles.

Figure 2 (top) shows the experimental XRD pattern obtained for our $BaGdF_5$ nanoparticles. All the reflections present match those of cubic $BaGdF_5$ (PDF 00-024-0098). However, our experimental reflections are slightly shifted towards higher angles, indicating a smaller unit cell parameter compared with that given in the mentioned PDF file (a= 6.023 Å). In order to calculate the unit cell dimensions of our particles, we have carried out a Rietveld refinement[30] of the structure using the TOPAS software (TOPAS version 4.2, Bruker AXS, 2009). Given that no description of the $BaGdF_5$ crystal structure could be found in the literature, we used, as starting parameters, those reported for $BaYF_5$ by Huang et al.,[26] who described the structure using the *Fm-3m* space group with a= 5.890 Å. The refined parameters were: scale, background coefficients, zero error, cubic unit cell parameter, and atomic displacement factors of the heavy atoms (Gd and Ba). The fitted curve, together with the difference one, is shown in Figure 2 (top). The unit cell parameter obtained was a= 5.9073(4) Å, which is in between those reported for $BaYF_5$ (a= 5.890 Å)[26] and $BaCeF_5$ (a= 6.033 Å).[31] These are the only two $BaLnF_5$ phases reported in the literature, in addition to the $BaGdF_5$ phase reported in PDF 00-024-0098, as commented above. We have plotted in Figure 2 (bottom) the unit cell volume of these two phases, plus those of the $BaGdF_5$ obtained in this work plus the one reported in ICDD 00-024-0098, versus the ionic radius of the corresponding Ln^{3+}. It can be observed that the R factor of the regression line calculated using the $BaGdF_5$ cell

volume of this work is significantly better (R= 0.95) that that obtained with the $BaGdF_5$ cell volume reported in ICDD 00-024-0098 (R= 0.76), indicating that ours represents a more reliable value.

Finally, it is noteworthy that the crystallite size obtained after applying the Scherrer formula to the 220 reflection (located at 43.3 °2θ) was 42 nm, which is very close to the particle dimension inferred from the TEM images. This result suggests that the particles are probably single crystals, which is highly desirable from an optical point of view due to the known fact that the luminescence efficiency increases with increasing the crystallinity perfection of the host matrix.[32]

3.3.- Synthesis and characterization of the Ln:$BaGdF_5$ nanoparticles (Ln= Eu^{3+} and Nd^{3+}).

With the aim of optimizing the luminescence properties of the $BaGdF_5$ nanophosphors doped with $Eu^{3+}$and Nd^{3+}, we synthesized different compositions of both phosphors, namely 2.5%, 5%, 10% and 20% Eu^{3+} in $BaGdF_5$ and 0.5%, 1.0%, and 1.5% Nd^{3+} in $BaGdF_5$. The differences in compositions used for each dopant are due to the known fact that concentration quenching for Nd^{3+} doped materials appear at much lower levels than in the case of Eu^{3+} doping.[33,34] The syntheses were carried out using the method reported above for the undoped material, and adding the corresponding amount of europium or neodymium acetylacetonate in each case. It was found that the shape, size and crystal structure of the undoped particles was reproduced for all doped samples irrespective of doping ions and doping levels (Figure S2, top and Figure S3, top). The XRD patterns of the doped Eu^{3+}:$BaGdF_5$ and Nd^{3+}:$BaGdF_5$ particles were very similar to the one of the undoped material (Figure S2, bottom and Figure S3, bottom). In both cases, the reflections were slightly shifted towards lower 2theta values, which indicated an increase in the unit cell size of the doped materials compared to the undoped particles. Such increase suggests that Gd^{3+} (ionic radius in VIII co-ordination= 1.053 Å) has been substituted by the bigger doping ions (Eu^{3+} ionic radius in VIII co-ordination= 1.066 Å[35] and Nd^{3+} ionic radius in VIII co-ordination= 1.109 Å[35]).

To confirm effective replacement of Gd^{3+} for Eu^{3+} and Nd^{3+} in the crystal structure of $BaGdF_5$ and the corresponding formation of the $BaGd_{1-x}Eu_xF_5$ and $BaGd_{1-x}Nd_xF_5$ solid solutions, the XRD patterns of the doped particles were analyzed by the Rietveld method to obtain the corresponding unit cell volumes. The values obtained have been

plotted in Figure 3, where a linear increase of the unit cell volume can be observed with increasing doping level in both cases, as expected from the different ionic radii of Gd^{3+} and each doping ion, as commented above. The observed behavior satisfies Vegard´s law[36] and indicates that Eu^{3+} and Nd^{3+} are replacing Gd^{3+} in each $BaGdF_5$ crystal structure. Finally, it is also worth mentioning that the comparison between the unit cell volumes obtained for the Eu- and Nd-doped materials is in good agreement with the bigger size of Nd^{3+} respect to Eu^{3+}.

3.4.- Luminescence of the Ln:BaGdF$_5$ (Ln= Eu^{3+} and Nd^{3+}) nanoparticles.

3.4.1.- Eu^{3+}-doped BaGdF$_5$ nanoparticles: The photoluminescence properties of the Eu^{3+}:$BaGdF_5$ nanoparticles with different Eu^{3+} contents were evaluated in order to find the optimum nanophosphor. The excitation spectrum recorded for 5% Eu^{3+}-containing sample by monitoring the Eu^{3+} emission at 593 nm (Figure 4a) displays a strong band at 273 nm along with much weaker features in the 300–400 nm range, among which the most intense appeared at 393 nm. The latter are due to the direct excitation of the Eu^{3+} ground state electrons to higher levels of the 4f-manifold, whereas the former can be ascribed to the electronic transition from the ground state level of Gd^{3+} ($^8S_{7/2}$) to the $^6I_{7/2\text{-}17/2}$ excited levels. The observation of this band while monitoring a Eu^{3+} emission indicates that an energy transfer from Gd^{3+} multiplets to Eu^{3+} electronic levels takes place in this sample.[37]

The excitation of the 5% Eu^{3+}-containing sample either at 273 or at 393 nm resulted (Figure 4b) in similar emission spectra composed of several bands, characteristic of transitions between the Eu^{3+} electronic levels, which have been labeled in the figure.[38] The intensity of the Eu^{3+} emissions was considerably higher when exciting through the Gd–Eu energy transfer band (λ_{ex} = 273 nm) than by direct excitation of the Eu^{3+} electronic levels (λ_{ex} = 393 nm), as expected from the excitation spectrum recorded for this sample and this wavelength will be used later on to analyse the influence of Eu concentration on the samples luminescence. The two dominant bands at 590 nm and 612 nm observed in Figure 4b are due to the $^5D_0$–$^7F_1$ and $^5D_0$–$^7F_2$ transitions, respectively, and they confer the sample an orange-red luminescence when irradiated with UV light at 273 or 393 nm (CIE coordinates: x= 0.57, y= 0.43 plotted in the inset of Figure 4b). The $^5D_0$–$^7F_1$ transition is due to the magnetic dipole transition of Eu^{3+} ions and it is independent on the symmetry of the Eu^{3+} site. However, the $^5D_0$–$^7F_2$

transition is a forced electric dipole transition, hypersensitive to the site symmetry of the Eu^{3+} ions. The lower intensity of the latter, observed in our spectrum, suggests that the Eu^{3+} ions are located at a centrosymmetric site,[39,40] in agreement with the *4a* site of the rare earth ion in the cubic (S.G. 225) $BaGdF_5$ crystal structure. Also noteworthy is the presence of a weaker band at lower wavelengths (554 nm) that is associated with the $^5D_1$–$^7F_2$ transition. The low phonon energy of the fluoride matrix is known to cause a low probability of quenching by multiphonon relaxation that explains the observation of such emission at low wavelengths.[41] The emission spectra of the rest of Eu compositions (Figure 4c) exhibit very similar bands to those of Figure 4b; the intensity of the emissions increased with increasing Eu^{3+} content up to 10% and then decreased for higher Eu doping levels. The scattered points in Figure 4d represent the integrated area of the spectra plotted in Figure 4c *vs.* Eu content. The curve obtained shows a clear deviation from a straight line indicating that the emission intensity is not directly proportional to the number of emission centers. This result suggests, therefore, the presence of a concentration quenching effect in most of the Eu-doped samples.

In order to gain additional information in this respect, luminescence lifetime measurements were carried out on the different Eu compositions using the excitation provided by the second harmonic of a pulsed Nd:YAG laser (λ_{exc} = 532 nm). This excitation efficiently populates the $^5D_1$ multiplet ($^7F_1 \rightarrow {}^5D_1$ transition) which then populates the $^5D_0$ state via non-radiative relaxation from where the different visible emissions originate (Figure S4).[39] It has been verified that the emission spectra under this excitation are coincident with that of Figure 4b, obtained after 273 nm or 393 nm excitation. The normalized temporal decays of the $^5D_0$ level, measured at the dominant Eu emission λ_{em} = 592 nm ($^5D_0 \rightarrow {}^7F_1$ transition), for the different Eu concentrations are shown in Figure 5 (top, dotted lines). After an initial rise, which corresponds to the filling of the $^5D_0$ emitting level from the upper $^5D_1$ level, as commented above, the luminescence curves showed an exponential decay. In the case of the low Eu-containing samples (2.5 and 5 %) such decay was successfully fitted to a single exponential decay of the form:

$$I(t) = I_0 \exp(-t/\tau) \qquad (1)$$

where *I(t) and* I_0 *= I(0)* are the luminescence intensity at time *t* and zero, respectively, *t* is the time after excitation and τ is the decay time. The luminescence curves of the

higher doped samples (Eu content= 10% and 20%) showed, however, a bi-exponential decay of the form:

$$I(t) = I_{01}\exp(-t/\tau_1)+I_{02}\exp(-t/\tau_2) \qquad (2)$$

where *I(t)* is the luminescence intensity, *t* is the time after excitation and τ_i *(i = 1, 2)* is the decay time of the *i*-component, with initial intensity I_{0i}. As reported for other fluoride-based particles, the long component could possibly be associated with the decay of Eu^{3+} ions located in the bulk, not affected by surface effects, whereas the shorter component could be ascribed to Eu^{3+} ions located nearer the surface of the nanoparticles, which could therefore be influenced by OH-species or surface defects that are known to act as luminescence quenchers.[33,42] The corresponding fitting curves have been plotted in Figure 5 (top, solid lines) while the fitting parameters are summarized in Table 1. Considering the non-exponential behavior of the decays, we have calculated the average life-time values, <τ>, defined as:

$$\langle\tau\rangle = \frac{\int_{t_0}^{t_f} tI(t)dt}{\int_{t_0}^{t_f} I(t)dt} = \left(\tau_1^2 I_1 + \tau_2^2 I_2\right)/\left(\tau_1 I_1 + \tau_2 I_2\right) \qquad (3)$$

where t_f represents a final time where the luminescence signal reaches the background, while t_0 represents a time delay after the excitation pulse from where the luminescence decay is analysed. This delay time has been chosen such to avoid the initial rise transient, and for that purpose a time $t_0 \approx 2\ t_M$, where t_M represents the time when the intensity reaches its maximum. This delay, which represents a minimum fraction of the total decay time, guarantees that the feeding from upper levels is excluded in the analysis.

For calculation purposes, the experimental decays have been fitted within these limits using the bi-exponential form given by eq. (2) (see the solid lines in Figure 5, top) and then, average lifetimes have been calculated from the corresponding fitting parameters (Table 1) using the right-hand side of eq. (3), which is readily derived assuming a bi-exponential decay.

These average lifetimes have been plotted, versus Eu^{3+} concentration, in Figure 5 (bottom). As observed, the emission lifetime remained almost constant (~11.5 ms) for the 2.5–5% Eu-containing samples and then decreased with increasing Eu doping level, reaching a value of 8.7 ms for the sample doped with 20% Eu^{3+}. These data confirm that a concentration quenching is present in the samples above Eu doping levels of 5% and that the most efficient Eu:$BaGdF_5$ nanophosphor is, therefore, the one doped with 5 mol% of Eu^{3+}. This is, to best of our knowledge, the first time that Eu^{3+} lifetime values in Eu:$BaGdF_5$ nanophosphors are reported in the literature, which precludes a comparative analysis of the luminescence efficiency of our nanophosphors with other previously reported. In particular, we cannot identify at this point the mechanism responsible of the observed concentration quenching. It is widely accepted that the luminescence of RE-doped nanoparticles is strongly influenced by the presence of some radicals, for instance OH- groups, both in the volume or in the surface, which act as "luminescence killers".[33,42] Therefore, a plausible mechanism responsible for the observed concentration quenching would be energy migration of the excitation between RE ions, which facilitates it could reach the proximity of killers, enhancing therefore the quenching of luminescence. But there are other possible options, such as direct "cross relaxation" between RE ions, an additional route for de-excitation that would increase when increasing dopant concentration and that may trigger also luminescence quenching. Both mechanisms are plausible (and perhaps concurrent), but they are only tentative proposals to be considered as underlying mechanisms responsible for the observed concentration quenching.

3.4.2.- Nd^{3+}-doped $BaGdF_5$ nanoparticles: The excitation spectrum of the 1.5%Nd^{3+}-doped $BaGdF_5$ nanophosphor recorded by monitoring the Nd^{3+} emission at 1055 nm is shown in Figure 6a. It exhibits two intense excitation bands at 797 nm and 866 nm, corresponding to the electronic excitation from the Nd^{3+}ground state ($^4I_{9/2}$) to the excited levels $^4F_{5/2}$:$^2H_{9/2}$ and $^4F_{3/2}$, respectively, as depicted in the Nd^{3+} energy level diagram of Figure S5. A third, low intensity excitation band can also be observed at ~753 nm, which is due to the electronic transition from the $^4I_{9/2}$ ground state to the high energy $^4F_{7/2}$:$^4S_{3/2}$ multiplet. The emission spectrum of the same nanophosphor recorded while exciting at 797.7 nm, using a Ti-zaphire laser, showed (Figure 6b) the emissions characteristic of Nd^{3+} centered at ~900 nm, ~1050 nm and ~1325 nm, corresponding to the transitions from the $^4F_{3/2}$ level to the $^4I_{9/2}$, $^4I_{11/2}$ and $^4I_{13/2}$ levels, respectively (Figure

S5). In order to establish the optimum Nd doping level, luminescence lifetime measurements were carried out on the $BaGdF_5$ nanoparticles doped with 0.5%, 1.0% and 1.5% Nd^{3+} using the excitation provided by the second harmonic of a pulsed Nd:YAG laser (λ_{exc} = 532 nm). This excitation efficiently populates the $^2G_{7/2}$ multiplet ($^4I_{9/2} \rightarrow {}^2G_{7/2}$ transition) which then populates the $^4F_{3/2}$ state via non-radiative relaxation from where the different NIR emissions originate, as observed also in the Nd^{3+} energy level diagram of Figure S5. The luminescence decay curves have been plotted in Figure 6c (symbols) for all three Nd^{3+}-doped samples (0.5%, 1.0% and 1.5% Nd^{3+}). Also in this case, as observed for the Eu^{3+}-doped samples, a rise in the luminescence intensity occurs at the very beginning of the detection period, which corresponds to the filling of the emitting $^4F_{3/2}$ level from the upper $^2G_{7/2}$ level. After reaching a maximum, the luminescence decays following a non-exponential behavior. The decay can be fitted using a bi-exponential temporal dependence (like that of equation (2)) for all three compositions in this case (solid lines in Figure 6c). The existence of two different time components can be assigned to the already reported fact that the Nd^{3+} ions doped in the nanoparticles are separated into two kinds: inside the core and near or at the surface.[43] The corresponding fitting parameters are summarized in Table 2 together with the average decay time, $<\tau>$, calculated using equation (3). As observed in the Table, the average lifetime values calculated for the three samples clearly decreased with increasing Nd^{3+} content, with a maximum of 244 μs at 0.5% Nd content. Therefore, a concentration quenching effect is present in the Nd-doped samples for doping levels above 0.5%, this concentration being, therefore, the optimum for luminescence purposes.

As far as we know, the lifetime of Nd^{3+} ions in $BaGdF_5$ has not been previously published, although it has been recently reported for a variety of other nanoparticles.[44] Although the comparison is difficult, considering that lifetimes are affected not only by the intrinsic radiative properties of Nd^{3+}, but also by the host nature or surface treatments, a general trend has been advanced, showing longer lifetimes in fluorides than in oxide nanoparticles, and attributed to higher phonon energies and hence greater non-radiative losses in the latter.[44] In the present case, the observed lifetime (244 μs for 0.5% Nd content) is substantially longer than that reported for other fluorides (123 μs in KYF_4 or 3 μs in $NaGdF_4$, for instance), which suggests a high quantum efficiency of

Nd^{3+} luminescence in $BaGdF_5$, though further evaluation would be needed for a more quantitative analysis.

3.5.- Magnetic relaxivity.

We have used the particles which showed the optimum Eu^{3+} and Nd^{3+} doping level in the luminescence studies to evaluate their corresponding longitudinal (r_1) and transversal (r_2) magnetic relaxivity, respectively. With this purpose, the longitudinal (T1) and transversal (T2) proton relaxation times were measured at different concentrations for both types of nanoparticles (5% Eu^{3+}- and 0.5% Nd^{3+}-doped $BaGdF_5$) in water at 298 K. The 1/T1 and 1/T2 values obtained were plotted as a function of Gd^{3+} concentration for the Eu^{3+} and Nd^{3+}-doped $BaGdF_5$ nanoparticles (Figure S6). The slopes of the curves gave the relaxivity values r_1 and r_2 shown in Table 3. The corresponding r_2/r_1 values were 4.88 and 3.78 for the 5% Eu^{3+} and 0.5% Nd^{3+}-doped $BaGdF_5$ nanoparticles, respectively. The fact that these r_2/r_1 values are lower than 5 suggests that these samples could be adequate for use as positive contrast agents, the Nd-doped particles being more interesting due to their higher r_1 value.[45] Comparison of these values with those of the literature require that the spectra are recorded under the same magnetic field and same temperature, among other parameters. To the best of our knowledge, only Zhao et al.[19] have reported relaxivity values for $BaGdF_5$ particles at 1.5 T, as is our case. Their r_1 value was 2.13, which is indeed higher than ours, but unfortunately, they did not report on the r_2 value, which prevents the full comparison of the magnetic data.

3.6.- Cytotoxicity test.

For cytotoxicity analyses, we have also used the particles which showed the optimum Eu^{3+} and Nd^{3+} doping levels in the luminescence studies. Both types of particles were submitted to biocompatibility studies by evaluating the viability of Vero cells with the MTT assay.[46] MTT (3-(4,5-dimethylthiazol-2-yl)-2,5-diphenyltetrazolium bromide) is a yellow, water soluble tetrazolium salt which can be converted into a water-insoluble dark-blue formazan by metabolically active cells. Formazan crystals can then be dissolved in an organic solvent such as dimethyl sulfoxide and quantified by measuring the absorbance of the solution at 550 nm. The resultant value is then related to the number of living cells. The metabolic activity and proliferation of cells were thus measured after 24 h of culture. The viability percentages for both doping ions were

higher than 80% for concentrations up to 0.25 mg/mL for both samples (Figure 7). These results are similar to those published for other $BaGdF_5$ nanoparticles and demonstrate the negligible toxicity effects of this type of particles.[47]

4.- Conclusions

Uniform and well dispersed spherical (40(5) nm diameter) nanoparticles were obtained after aging, at 120 °C for 10 hours in a conventional furnace, 4 mL of a solution containing $Gd(acac)_3$ (0.12 M) and $Ba(NO_3)_3$ (0.12 M) in glycerol admixed with 2 mL of a glycerol solution of $[BMIM]BF_4$ (0.55 M). Changing anyone of the experimental conditions and keeping the rest constant, led to the loss of the dispersion, uniformity and/or morphology of the particles. Only the increase in cations (Ba^{2+} and Gd^{3+}) concentrations allowed obtaining uniform, spherical particles whose diameter exponentially increased with decreasing cations concentration. The obtained nanoparticles crystallized in the cubic system and exhibited a high degree of crystallinity with cubic cell parameter =5.9073(4) Å. The synthesis procedure was also successful for the preparation of Eu^{3+}- and Nd^{3+}-doped $BaGdF_5$ nanoparticles with the same morphology and crystalline structure as the undoped materials. The former showed a strong orange-red luminescence under near-UV excitation (393 nm), while the Nd^{3+}-doped particles exhibited near infrared luminescence when excited at 797 nm. The optimum doping levels, obtained from luminescence decay curves, were 5% and 0.5% for the Eu^{3+}- and Nd^{3+}-doped particles, respectively. Because of these properties these particles could be useful for optical imaging. In addition, these particles exhibited r_2/r_1 values lower than 5, which make them suitable for use as positive contrast agents in MRI imaging. Finally, these multifunctional probes have been found to be non-toxic for cells, fulfilling one of the requirements for their biotechnological applications.

Supporting information

TEM micrographs of $BaGdF_5$ samples prepared using diferente experimental conditions. SEM micrographs of $BaGdF_5$ particles doped with 2.5%, 5%, 10% and 20% Eu^{3+}. XRD patterns of the $BaGdF_5$ particles undoped and doped with 2.5%, 5%, 10% and 20% Eu^{3+}. SEM images of the 0.5% and 1.5 % Nd^{3+}: $BaGdF_5$ particles. XRD patterns of the $BaGdF_5$ particles undoped and doped with 0.5%, 1%, and 1,5% Nd^{3+}. Electronic energy levels of Eu^{3+} ion illustrating the excitation and emission processes. Electronic energy levels of Nd^{3+} ion illustrating the excitation and emission processes. Inverse of proton

relaxation times (1/T1 and 1/T2) of 5% Eu^{3+}- and 0.5%Nd^{3+}-doped $BaGdF_5$ nanoparticles in water suspensions as a function of Gd content.

Acknowledgements

Supported by MINECO (Project.MAT2014-54852-R and MAT2012-34919), CSIC (201460E005 and 201560E056) and ERC-Starting Grant NANOPUZZLE. M. C. Jiménez is gratefully acknowledged for help with *SEM*.

References

(1) Zhou, J.; Liu, Q.; Feng, W.; Sun, Y.; Li, F. Upconversion Luminescent Materials: Advances and Applications. *Chem. Rev.* **2015**, *115*, 395−465.

(2) Li, X.; Zhang, F.; Zhao, D. Highly efficient lanthanide upconverting nanomaterials: Progresses and challenges. *Nano Today* **2013**, *8*, 643-676.

(3) Chatterjee, D. K.; Gnanasammandhan, M. K.; Zhang, Y. Small Upconverting Fluorescent Nanoparticles for Biomedical Applications. *Small* **2010**, *6*, 2781-2795.

(4) Naccache, R.; Yu, Q.; Capobianco, J. A. The Fluoride Host: Nucleation, Growth, and Upconversion of Lanthanide-Doped Nanoparticles. *Adv. Opt. Mater*. **2015**, *3*, 482-509.

(5) Chen, H.; Lang, Y. B.; Zhang, Y. L.; Zhao, D.; Qin, G. S.; Wu, C. F.; Zheng, K. Z.; Qin, W. P. Dual mode emission of core-shell rare earth nanoparticles for fluorescence encoding. *J. Mater. Chem. C*, **2015**, *3*, 6314-6321.

(6) Diamente, P. R.; Raudsepp, M.; van Veggel, F. C. J. M. Dispersible Tm^{3+}-doped nanoparticles that exhibit strong 1.47 mu m photoluminescence. *Adv. Func. Mater.* **2007**, *17*, 363-368.

(7) Renero-Lecuna, C.; Martín-Rodríguez, R.; Valiente, R.; González, J.; Rodríguez, F.; Kramer, K. W.; Gudel, H. U. Origin of the High Upconversion Green Luminescence Efficiency in beta-NaYF4:2%Er3+,20%Yb3+. *Chem. Mater.* **2011**, *23*, 3442-3448.

(8) Yang, L.W.; Zhang, Y. Y.; Li, J. J.; Li, Y.; Zhong, J. X.; Chu, P. K. Magnetic and upconverted luminescent properties of multifunctional lanthanide doped cubic KGdF4 nanocrystals. *Nanoscale* **2010**, *2*, 2805-2810.

(9) Naccache, R.; Chevallier, P.; Lagueux, J.; Gossuin, Y.; Laurent, S.; Vander Elst, L.; Chilian, C.; Capobianco, J. A.; Fortin, M. A. High Relaxivities and Strong Vascular Signal Enhancement for NaGdF4 Nanoparticles Designed for Dual MR/Optical Imaging. *Adv. Healthcare Mater.* **2013**, *2*, 1478-1488.

(10) Banski, M.; Afzaal, M.; Cha, D.; Wang, X.; Tan, H.; Misiewicz, J.; Podhorodecki, A. Crystal phase transition in $Li_xNa_{1-x}GdF_4$ solid solution nanocrystals - tuning of optical properties. *J. Mater. Chem. C* **2014**, *2*, 9911-9917.

(11) Duhnen, S.; Rinkel, T.; Haase, M. Size Control of Nearly Monodisperse beta-$NaGdF_4$ Particles Prepared from Small alpha-NaGdF4 Nanocrystals. *Chem. Mater*. **2015**, *27*, 4033 – 4039.
(12) Wong, H. T.; Tsang, M. K.; Chan, C. F.; Wong, K. L.; Feic, B.; Hao, J. In vitro cell imaging using multifunctional small sized $KGdF_4:Yb^{3+},Er^{3+}$ upconverting nanoparticles synthesized by a one-pot solvothermal process. *Nanoscale* **2013**, *5*, 3465-3473.
(13) Yang, D.; Li, C.; Li, G.; Shang, M.; Kang, X.; Lin, J. Colloidal synthesis and remarkable enhancement of the upconversion luminescence of $BaGdF_5:Yb^{3+}/Er^{3+}$ nanoparticles by active-shell modification. *J. Mater. Chem*. **2011**, *21*, 5923-5927.
(14) Zhang, C.; Wang, J.; Song, C.; Shang, Y.; Shen, S. BaGdF5:Ce3+, Ln(3+) (Ln=Eu and Tb) nanoparticles: Tunable multicolor emission and magnetic property. *Mater. Letters* **2014**, *118*, 88-91.
(15) Guo, L.; Wang, Y.; Wang, Y.; Zhang, J.; Dong, P. Crystal structure and up- and down- conversion properties of Yb^{3+}, Ho^{3+} codoped $BaGdF_5$ solid-solution with different morphologies. *CrystEngComm* **2012**, *14*, 3131-3141.
(16) Grzyb, T.; Mrówczy´nska, L.; Szczeszak, A.; Sniadecki, Z.; Runowski, M.; Idzikowski, B.; Lis, S. Synthesis, characterization and cytotoxicity in human erythrocytes of multifunctional, magnetic, and luminescent nanocrystalline rare earth fluorides. *J. Nanopart. Res.* **2015**, *17*, 399-416.
(17) Zeng, S.; Tsang, M.; Chan, C.; Wong, K.; Hao, J. PEG modified BaGdF5:Yb/Er nanoprobes for multi-modal upconversion fluorescent, in vivo X-ray computed tomography and biomagnetic imaging. *Biomaterials* **2012**, *33*, 9232-9238.
(18) Yang, D.; Kang, X.; Shang, M.; Li, G.; Peng, C.; Li, C.; Lin, L. Size and shape controllable synthesis and luminescent properties of BaGdF5: Ce3+/Ln(3+) (Ln = Sm, Dy, Eu, Tb) nano/submicrocrystals by a facile hydrothermal process. *Nanoscale* **2011**, *3*, 2589-2595.
(19) Zhao, Q.; Lei, Z.; Huang, S.; Han, X.; Shao, B.; Lü, W.; Jia, Y.; Lv, W.; Jiao, M.; Wang, Z.; You, H. Facile Fabrication of Single-Phase Multifunctional BaGdF5 Nanospheres as Drug Carriers. *ACS Appl. Mater. Interfaces* **2014**, *6*, 12761-12770.
(20) Sarkar, S.; Hazra, C.; Mahalingam, V. Scaling down the size of BaLnF(5) nanocrystals (Ln = La, Gd, and Lu) with the Ln(3+) size. *Dalton Trans.* **2013**, *42*, 63-66.
(21) Nuñez, N.O.; Quintanilla, M.; Cantelar, E.; Cussó, F.; Ocaña, M. Uniform YF3:Yb,Er up-conversion nanophosphors of various morphologies synthesized in polyol media through an ionic liquid. *J. Nanopart. Res.* **2010**, *12*, 2553–2565.
(22) Rodriguez-Liviano, S.; Nuñez, N. O.; Rivera-Fernández, S.; de la Fuente, J. M.; Ocaña, M. Ionic Liquid Mediated Synthesis and Surface Modification of Multifunctional Mesoporous Eu:GdF3 Nanoparticles for Biomedical Applications. *Langmuir* **2013**, *29*, 3411−3418.
(23) Becerro, A. I.; Criado, J.; Gontard, L. C.; Obregón, S.; Fernández, A.; Colón, G.; Ocaña, M. Bifunctional, Monodisperse $BiPO_4$-Based Nanostars: Photocatalytic Activity and Luminescent Applications. *Cryst. Growth Des.* **2014**, *14*, 3319−3326.

(24) Naccache, R.; Vetrone, F.; Mahalingam, V.; Cuccia, L. A.; Capobianco, J. A. Controlled Synthesis and Water Dispersibility of Hexagonal Phase $NaGdF_4:Ho^{3+}/Yb^{3+}$ Nanoparticles. *Chem. Mater.* **2009**, *21*, 717-723.
(25) Rocha, U.; Kumar, K. U.; Jacinto, C.; Villa, I.; Sanz-Rodríguez, F.; Iglesias de la Cruz, M.; Juarranz, A.; Carrasco, E.; van Veggel, F. C. J. M.; Bovero, E.; García Solé, J.; Jaque, D. Neodymium-Doped LaF_3 Nanoparticles for Fluorescence Bioimaging in the Second Biological Window. *Small* **2014**, *10*, 1141-1154.
(26) Huang, Y. J.; You, H. P.; Jia, G.; Song, Y. H.; Zheng, Y. H.; Yang, M.; Liu, K.; Guo, N. Hydrothermal Synthesis, Cubic Structure, and Luminescence Properties of $BaYF_5$:RE (RE = Eu, Ce, Tb) Nanocrystals. *J. Phys. Chem. C* **2010**, *114*, 18051-18058.
(27) LaMer, V. K.; Dinegar, R. H. Theory, production and mechanism of formation of monodispersed hydrosols. *J. Am. Chem. Soc*. **1950**, *72*, 4847-4854.
(28) Matijevic, E. Preparation and properties of uniform size colloids. *Chem. Mater.* **1993**, *5*, 412-419.
(29) Duan, X.; Li, Y. Physicochemical Characteristics of Nanoparticles Affect Circulation, Biodistribution, Cellular Internalization, and Trafficking. *Small* **2013**, *9*, 1521-1532.
(30) Rietveld, H. M. A profile refinement method for nuclear and magnetic structures. *J. Appl. Crystallogr*. **1969**, *2*, 65-71.
(31) Aleksandrov, V. B.; Otroshchenko, L. P. ; Fykin, L. E.; Bydanov, N. N.; Sobolev, B. P. Features of defect structure of CeF_3 saturated fluorite solid-solution of $Ba_{0.5}Ge_{0.5}F_{2.5}$ from neutron-diffraction data on single-crystals. *Kristallografiya* **1989**, *34*, 1497-1501.
(32) Pan, Y.; Wu, M.; Su, Q. Comparative investigation on synthesis and photoluminescence of YAG : Ce phosphor. *Mater. Sci. Eng. B* **2004**, *106*, 251–256.
(33) Becerro, A. I.; Rodríguez-Liviano, S.; Fernández-Carrión, A. J.; Ocaña, M. A Novel 3D Architecture of $GdPO_4$ Nanophosphors: Multicolored and White Light Emission. *Crystal Growth & Design* **2013**, *13*, 526-535.
(34) Wang, Q.; Qiu, J. B.; Song, Z. G.; Yang, Z. W.; Yin, Z. Y.; Zhou, D. C. Optical properties of Ce^{3+}-Nd^{3+} co-doped YAG nanoparticles for visual and near-infrared biological imaging. *Spectrochim. Acta A* **2015**, *149*, 898‑903.
(35) Shannon, R. D. Revised effective ionic-radii and systematic studies of interatomic distances in halides and chalcogenides. *Acta Cryst. A* **1976**, *32*, 751-767.
(36) Vegard, L. The constitution of the mixed crystals and the filling of space of the atoms. *Z. fur Physik* **1921**, *5*, 17-26.
(37) Fernández-Carrión, A. J.; Ocaña, M.; García-Sevillano, J.; Cantelar, E.; Becerro, A. I. New Single-Phase, White-Light-Emitting Phosphors Based on delta-Gd2Si2O7 for Solid-State Lighting. *J. Phys. Chem. C* 2014**, 118**, 18035−18043.
(38) Karbowiak, M.; Mech, A.; Bednarkiewicz, A.; Strek, W.; Kepinski, L. Comparison of different $NaGdF_4:Eu^{3+}$ synthesis routes and their influence on its structural and luminescent properties. *J. Phys. Chem. Solids* **2005**, *66*, 1008-1019.
(39) Blasse, G.; Grabmaier, B. C. **1994**, Luminescent materials. Springer, Berlin.

(40) Tanner, P. A. Some misconceptions concerning the electronic spectra of tri-positive europium and cerium. *Chem. Soc. Rev.* **2013**, *42*, 5090–5101.
(41) Hölsä, J.; Kestilä, E. Crystal fields in REOF - Eu^{3+} (RE=La, Gd and Y). *J. Chem. Soc. Faraday Trans.* **1995**, *91*, 1503-1509.
(42) Sayed, F. N.; Grover, V.; Dubey, K. A.; Sudarsan, V.; Pandey, B. N.; Asthana, A.; Vatsa, R. K.; Tyagi, A. K. Multicolored and white-light phosphors based on doped GdF_3 nanoparticles and their potential bio-applications. *J. Colloid Interf. Sci.* **2012**, *367*, 161-170.
(43) Stouwdam, J. W.; van Veggel, F. C. J. M. Near-infrared emission of redispersible Er^{3+}, Nd^{3+}, and Ho^{3+} doped LaF_3 nanoparticles. *Nano Lett.* **2002**, *2*, 733–737.
(44) del Rosal, B.; Pérez-Delgado, A.; Misiak, M.; Bednarkiewicz, A.; Vanetsev, A.S.; Orlovskii, Y.; Jovanovic, D.J.; Dramicanin, M. D.; Rocha, U.; Kumar, K. U.; Jacinto, C.; Navarro, E.; Martín Rodríguez, E.; Pedroni, M.; Speghini, A.; Hirata, G. A.; Martín, I. R.; Jaque, D. Neodymium-doped nanoparticles for infrared fluorescence bioimaging: The role of the host. J. Appl. Phys. **2015**, *118*, 143104.
(45) Peng, E.; Wang, F.; Xue, J. M. Nanostructured magnetic nanocomposites as MRI contrast agents. *J. Mater., Chem. B* **2015**, *3*, 2241-2276.
(46) Mosmann, T. Rapid colorimetric assay for cellular growth and survival - application to proliferation and cyto-toxicity assays. *J. Immunol. Methods* **1983**, *65*, 55-63.
(47) Zhang, H.; Wu, H.; Wang, J.; Yang, Y.; Wu, D.; Zhang, Y.; Zhang, Y.; Zhou, Z.; Yang, S. Graphene oxide-BaGdF5 nanocomposites for multi-modal imaging and photothermal therapy. Biomaterials 2015, 42, 66-77.

Table 1: Fitting parameters of the single and bi-exponential temporal dependence for the luminescence decay curves of the Eu^{3+}-doped $BaGdF_5$ nanophosphors recorded at the dominant emission of the Eu^{3+} ion. The average lifetime <□> has been calculated from the right hand-side term of equation (3), using the corresponding fitting parameters.

%Eu^{3+}	**I_{01}**	**τ_1 (ms)**	**I_{02}**	**τ_2 (ms)**	**<τ> (ms)**
2.5	1.00	11.3			11.3
5	1.00	11.5			11.5
10	0.88	10.8	0.12	3.9	10.5
20	0.83	9.2	0.17	2.87	8.8

Table 2: Fitting parameters of the bi-exponential temporal dependence for the luminescence decay curves of the Nd^{3+}-doped $BaGdF_5$ nanophosphors recorded at the dominant emission of the Nd^{3+} ion. The average lifetime <□> has been calculated from the right hand-side term of equation (3), using the corresponding fitting parameters

%Nd^{3+}	**I_{01}**	**τ_1(μs)**	**I_{02}**	**τ_2 (μs)**	**<τ> (μs)**
0.5	0.62	78	0.38	312	244
1.0	0.67	83	0.33	312	232
1.5	0.72	84	0.28	312	219

Table 3: Proton relaxivity values (r_1 and r_2) obtained for water suspensions of the Ln-doped BaGdF5 nanoparticles at 1.5 T and 298 K.

Ln-$BaGdF_5$ nanoparticles	**r1** (**s^{-1} mM^{-1}**)	**r2** (**s^{-1} mM^{-1}**)	**r2/r1**
5% Eu^{3+}	0.59	2.88	4.88
0.5% Nd^{3+}	0.93	3.52	3.78

Figure captions:

Figure 1: *Top:* TEM micrograph showing uniform spherical (~40 nm diameter) nanoparticles obtained after aging, at 120 °C for 10 hours in a conventional furnace, a solution containing $Gd(acac)_3$ (0.12 M) and $Ba(NO_3)_3$ (0.12 M) in glycerol admixed with 2 mL $[BMIM]BF_4$ (0.55 M). *Middle*: Hydrodynamic diameter distribution, obtained from DLS technique on an aqueous suspension of the particles shown in the left. *Bottom*: Exponential decay of the average diameter of the particles with increasing Gd^{3+} and Ba^{2+} concentrations. The average diameter was calculated from TEM micrographs The solid line is the exponential fit to the data. Error bars represent the standard deviation of the measurement.

Figure 2: *Top:* Experimental (crosses) and fitted (solid line) XRD pattern of the $BaGdF_5$ particles shown in Figure 2b. *Bottom: U*nit cell volume of different $BaLnF_5$ compounds versus the Ln^{3+} ionic radius: $BaYF_5$,[26] $BaCeF_5$,[31] and $BaGdF_5$ (values from PDF 00-024-0098 and from this work). The solid red line is the linear fit to the red data points while the dashed blue line is the linear fit to the data points corresponding to $BaYF_5$, $BaCeF_5$ and $BaGdF_5$ from this work.

Figure 3: Unit cell volume of the Ln:$BaGdF_5$ (Ln= Eu^{3+} and Nd^{3+}) particles versus Ln content. Different x-axes have been used for the Nd^{3+} and Eu^{3+}-doped samples due to their different doping levels.

Figure 4: *a)* Excitation spectrum of the 5% Eu^{3+}-doped $BaGdF_5$ nanoparticles recorded at the characteristic Eu^{3+} emission wavelength of 593 nm. *b)* Emission spectra of the 5% Eu^{3+}-doped $BaGdF_5$ nanoparticles recorded after excitation at 273 nm and 393 nm. The inset is *a* CIE diagram showing the coordinates obtained for an aqueous suspension of the nanoparticles illuminated at 393 nm. *c)* Emission spectra of the different Eu-doped samples after exciting at λ_{ex}=273 nm. *d)* Integrated area (circles) of the spectra shown above versus Eu content.

Figure 5: *Top:* Temporal evolution of the $^5D_0$–$^7F_1$ luminescence for the $BaGdF_5$ nanophosphors doped with different amounts of Eu^{3+} (excitation at 532 nm). Solid lines correspond to the fitting of the experimental data using equations (1) (Eu content = 2.5

and 5 %) or equation (2) (Eu content = 10 and 20 %) with the parameters given in Table 2. *Bottom:* Evolution of the average lifetimes with Eu^{3+} content.

Figure 6: *a)* Excitation spectrum of the 1.5% Nd^{3+}-doped $BaGdF_5$ nanoparticles recorded by monitoring the Nd^{3+} emission at 1055 nm. *b)* Emission spectrum of the 1.5% Nd^{3+}-doped $BaGdF_5$ nanophosphor recorded while exciting at 797.7 nm, using a Ti-zaphire laser. *c)* Temporal evolution of the $^4F_{3/2} - {}^4I_{11/2}$ luminescence for the $BaGdF_5$ nanophosphors doped with different amounts of Nd^{3+} (excitation at 532 nm using the 2^{nd} harmonics of a Nd:YAG laser). Solid lines correspond to the fitting of the experimental data assuming a bi-exponential luminescence decay, using equation (2) with the parameters given in Table 2.

Figure 7: Cytotoxicity profiles of 5% Eu^{3+} and 0.5%Nd^{3+}-doped $BaGdF_5$ nanoparticles (top and bottom, respectively) with Vero cells, determined by MTT assay. Percentage of viability of cells was expressed relative to control cells (n = 5). Results are represented as mean ± standard deviations.

Figure 1

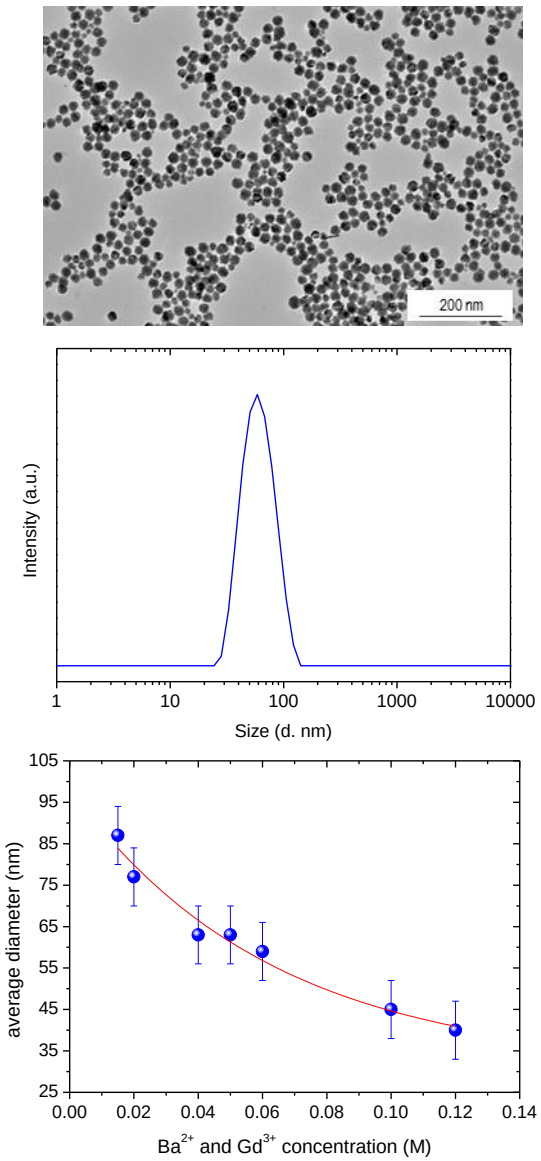
200 nm
Intensity (a.u.)
1
10
100
1000
10000
Size (d. nm)
105
95
85
75
65
55
45
35
25
average diameter (nm)
0.00
0.02
0.04
0.06
0.08
0.10
0.12
0.14
Ba2+ and Gd3+ concentration (M)

Figure 2

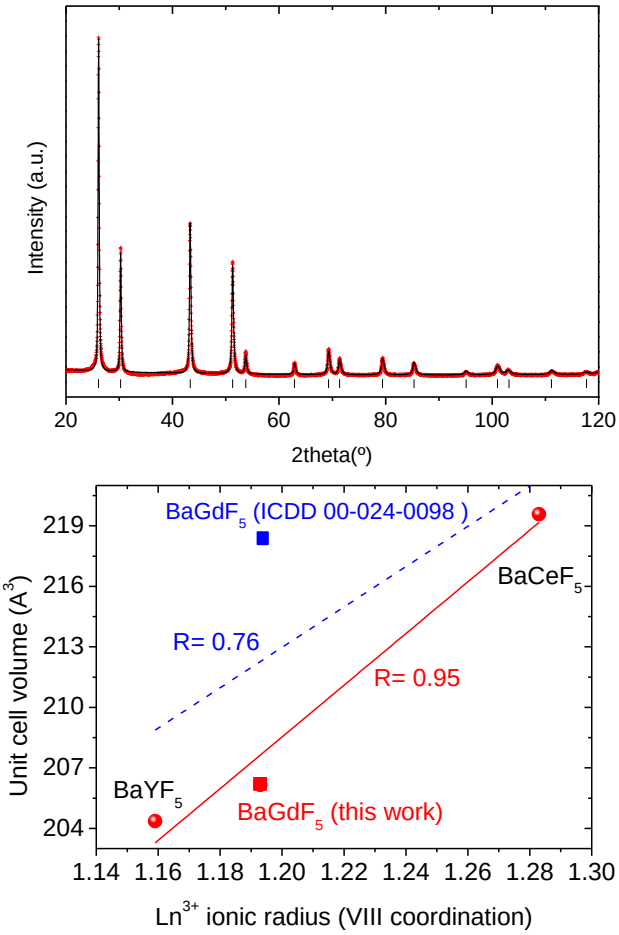
Intensity (a.u.)
20
40
60
80
100
120
2theta(º)
BaGdF5 (ICDD 00-024-0098)
BaCeF5
R= 0.76
R= 0.95
BaYF5
BaGdF5 (this work)
Unit cell volume (A3)
219
216
213
210
207
204
1.14
1.16
1.18
1.20
1.22
1.24
1.26
1.28
1.30
Ln3+ ionic radius (VIII coordination)

Figure 3

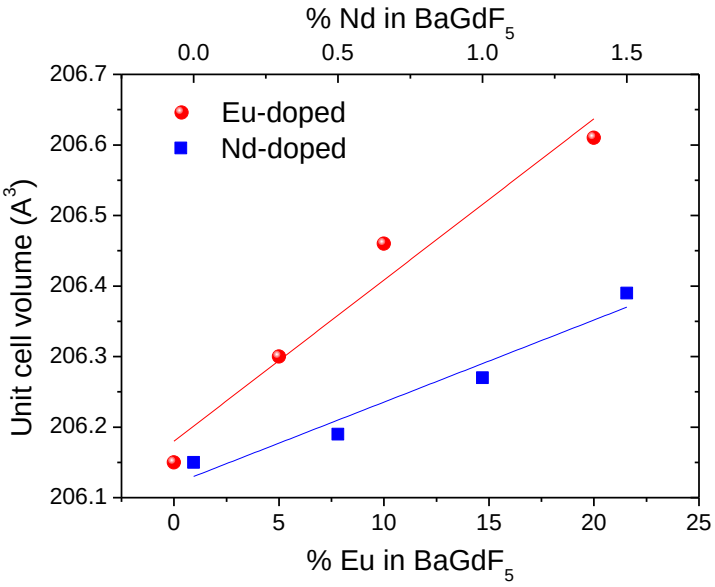
% Nd in BaGdF5
0.0
0.5
1.0
1.5
206.7
206.6
206.5
206.4
206.3
206.2
206.1
Unit cell volume (A3)
Eu-doped
Nd-doped
0
5
10
15
20
25
% Eu in BaGdF5

Figure 4

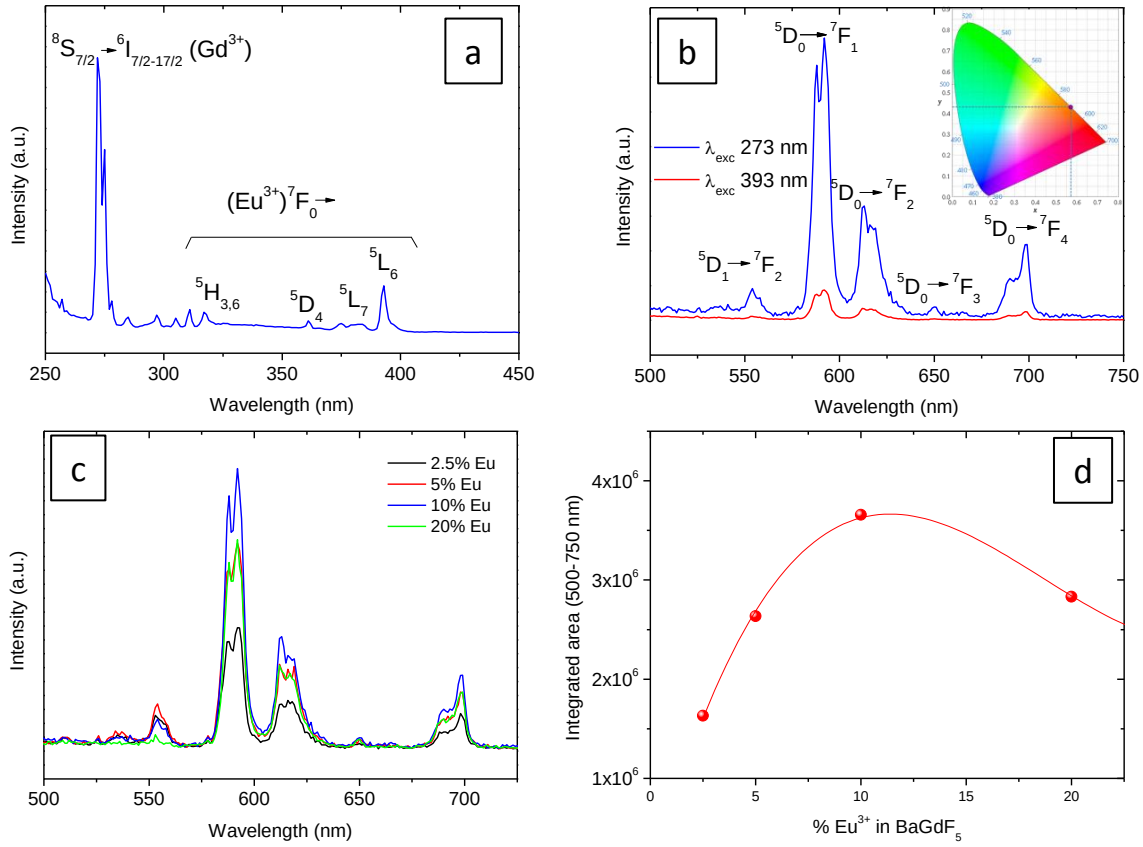
a
$^8S_{7/2} \rightarrow {}^6I_{7/2\text{-}17/2}$ (Gd^{3+})
$(Eu^{3+})^7F_0 \rightarrow$
$^5H_{3,6}$
$^5D_4$
$^5L_7$
$^5L_6$
Intensity (a.u.)
Wavelength (nm)
b
$^5D_0 \rightarrow {}^7F_1$
λ_{exc} 273 nm
λ_{exc} 393 nm
$^5D_0 \rightarrow {}^7F_2$
$^5D_0 \rightarrow {}^7F_4$
$^5D_1 \rightarrow {}^7F_2$
$^5D_0 \rightarrow {}^7F_3$
Intensity (a.u.)
Wavelength (nm)
c
2.5% Eu
5% Eu
10% Eu
20% Eu
Intensity (a.u.)
Wavelength (nm)
d
Integrated area (500-750 nm)
% Eu^{3+} in $BaGdF_5$

Figure 5

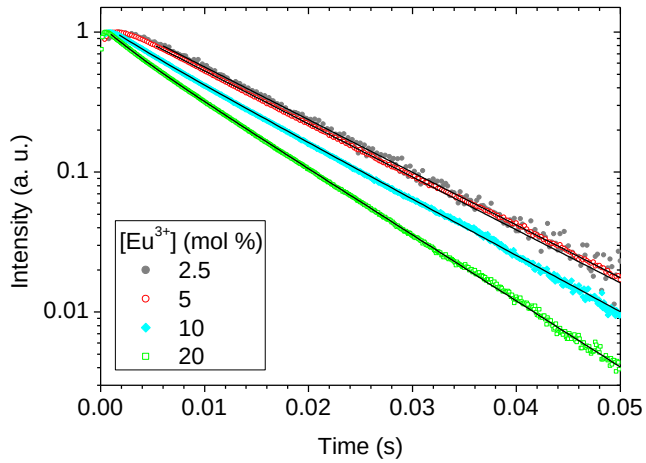
Intensity (a. u.)
1
0.1
0.01
0.00
0.01
0.02
0.03
0.04
0.05
Time (s)
[Eu3+] (mol %)
2.5
5
10
20

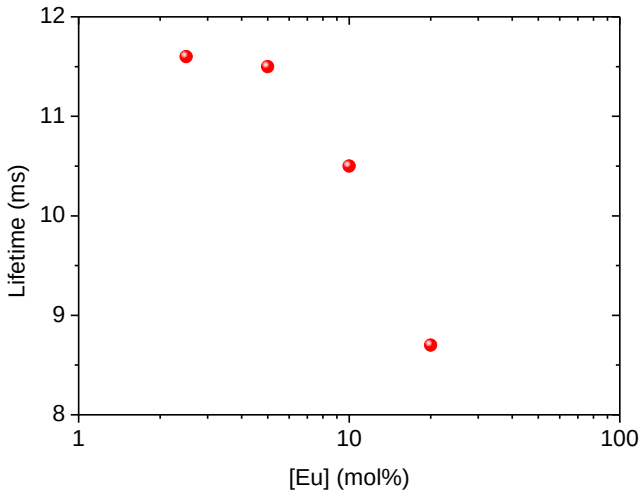
Lifetime (ms)
12
11
10
9
8
1
10
100
[Eu] (mol%)

Figure 6

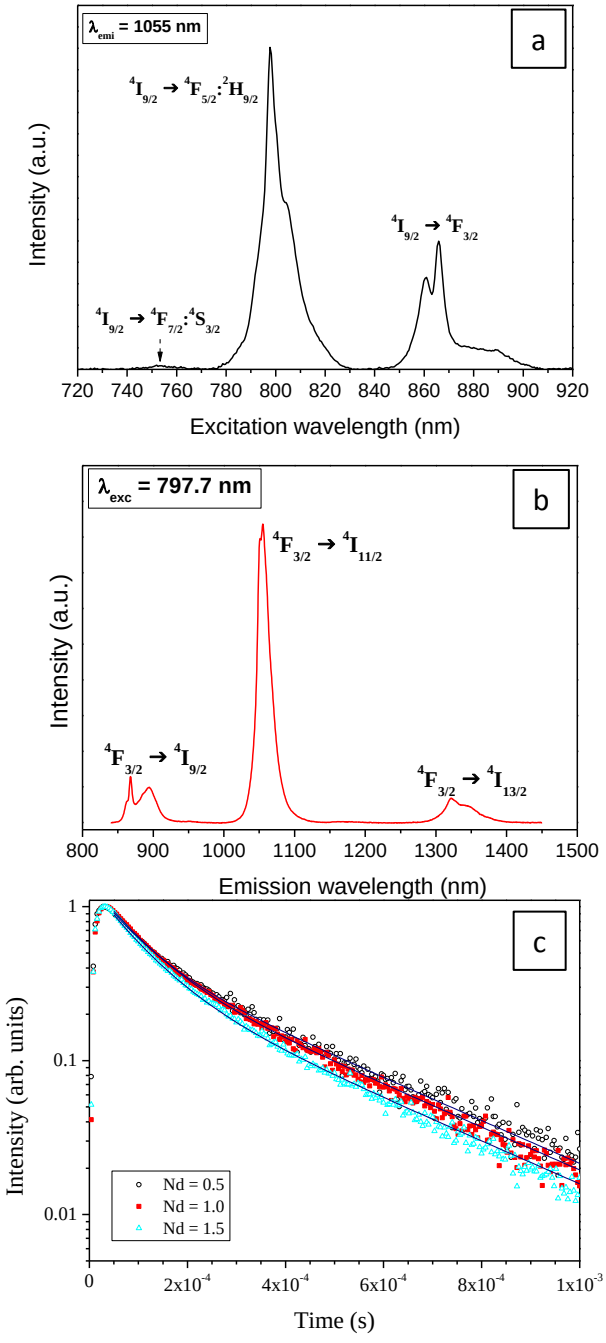
a
λemi = 1055 nm
4I9/2 → 4F5/2:2H9/2
4I9/2 → 4F3/2
4I9/2 → 4F7/2:4S3/2
Intensity (a.u.)
720 740 760 780 800 820 840 860 880 900 920
Excitation wavelength (nm)
b
λexc = 797.7 nm
4F3/2 → 4I11/2
4F3/2 → 4I9/2
4F3/2 → 4I13/2
Intensity (a.u.)
800 900 1000 1100 1200 1300 1400 1500
Emission wavelength (nm)
c
Nd = 0.5
Nd = 1.0
Nd = 1.5
Intensity (arb. units)
1
0.1
0.01
0
2x10-4
4x10-4
6x10-4
8x10-4
1x10-3
Time (s)

Figure 7

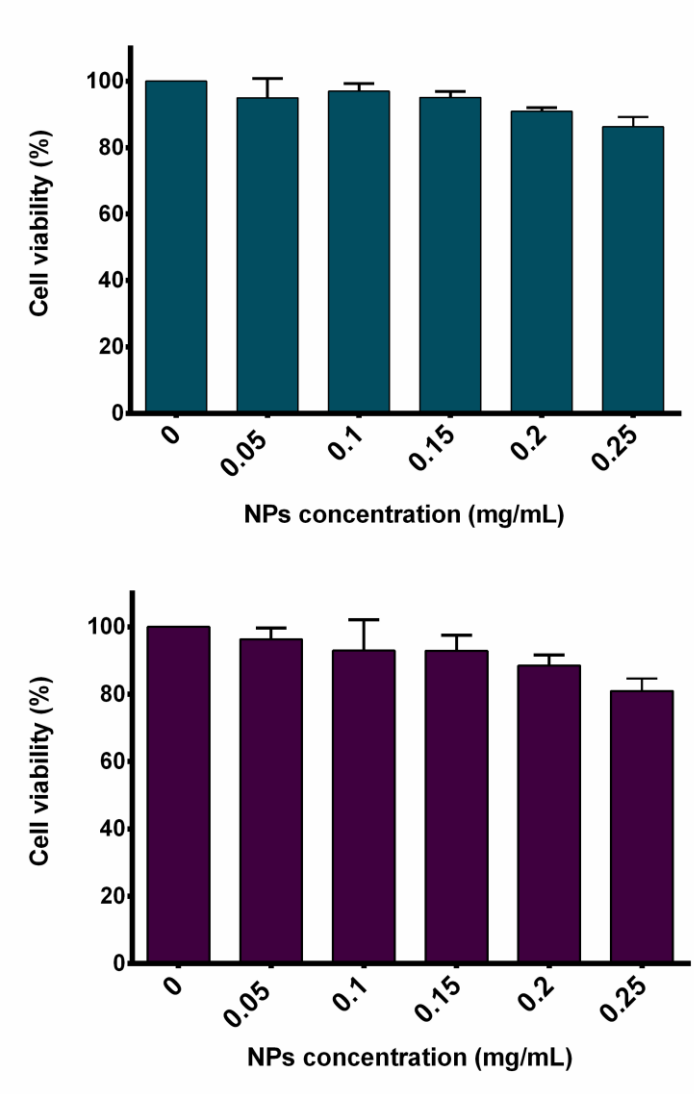
Cell viability (%)
100
80
60
40
20
0
0
0.05
0.1
0.15
0.2
0.25
NPs concentration (mg/mL)
Cell viability (%)
100
80
60
40
20
0
0
0.05
0.1
0.15
0.2
0.25
NPs concentration (mg/mL)

TOC Graphic

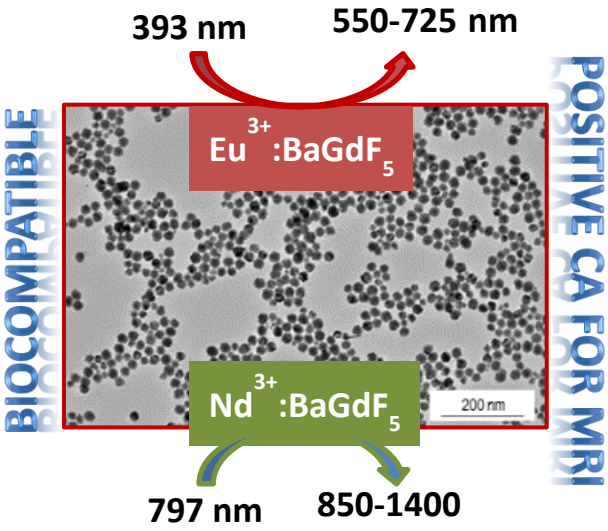
393 nm
550-725 nm
BIOCOMPATIBLE
POSITIVE CA FOR MRI
Eu3+:BaGdF5
Nd3+:BaGdF5
200 nm
797 nm
850-1400